

# Quasi-static probes of the QCD plasma

Debasish Banerjee,\* Rajiv V. Gavai,† and Sourendu Gupta‡

*Department of Theoretical Physics,  
Tata Institute of Fundamental Research,  
Homi Bhabha Road, Mumbai 400005, India.*

Screening correlators and masses were studied at finite temperature in QCD with two flavours of dynamical staggered quarks on a lattice. The spectrum of screening masses show a hierarchical approach to chiral symmetry restoration. Control of explicit chiral symmetry breaking through the quark mass was shown to be an important step to understanding this phenomenon. No sign of decays was found in the finite temperature scalar meson-like correlators in the confined phase.

PACS numbers: 12.38.Mh, 11.15.Ha, 12.38.Gc

## I. INTRODUCTION

High temperature QCD is the subject of a long-running experimental program of heavy-ion collisions in several experimental facilities, including the Relativistic Heavy Ion Collider (RHIC) at BNL, the Large Hadron Collider (LHC) at CERN, and planned programs in GSI and Dubna. They aim to collide together heavy-ions at high energies and produce fireballs of strongly interacting matter, whose study may then yield information about the phases and properties of such matter. Lattice computations are the primary source of theoretical information on such matter. The aim of this study is to examine the response of this matter to quasi-static perturbations.

It is known that the generic response of matter to such perturbations is to screen them. The knowledge of screening lengths,  $\xi$ , is one of the most basic pieces of microscopic information we can have about the system. Of particular interest is the longest screening length,  $\xi_0$ , or its inverse, the smallest screening mass,  $\mu_0 = 1/\xi_0$  [1]. When  $\mu_0 = 0$ , the effective long-distance theory of matter (at, or close to, equilibrium) requires us to take into account these unscreened perturbations. Such is the case in a QED plasma, where magnetic fields are not screened. Not only are equilibrium properties of a plasma strongly influenced by this, but also the off-equilibrium long-distance theory changes to magneto hydrodynamics rather than Navier-Stokes hydrodynamics, as it is for other fluids.

For the QCD plasma with non-vanishing quark masses, one knows that all fields are screened and the long-distance theory will be hydrodynamics coupled to the diffusion of conserved charges. Nevertheless, the study of screening masses is of practical importance. If the smallest dimension of the fireball produced in heavy-ion collisions is  $\ell$ , one expects thermodynamic properties to manifest themselves only when  $\ell\mu_0 \gg 1$ . Furthermore, since both these quantities are functions of the temperature  $T$ , it is possible for the fireball to drop into, and out of, equilibrium at different temperatures. In this way, quasi-static properties such as the screening masses may put bounds on truly dynamical quantities such as the thermalization and freezeout times in heavy-ion collisions.

The study of screening properties in a plasma has a long history. In the glue sector, the Debye screening length has been the object of many studies and now seems to be quantitatively understood, both in non-perturbative lattice studies [2] and in weak coupling theory at high temperatures [3]. Screening in other quantum number channels in the glue sector has also been studied [4]. Screening in colour singlet channels due to quark bilinear (meson-like) and trilinear (baryon-like) currents [1] was understood as the first signal of deconfinement above the chiral symmetry restoring temperature in QCD with dynamical quarks [5]. Analyticity arguments relate these hadron-like screening masses in the low-temperature confined and chiral symmetry broken phase to the (pole) masses and properties of the hadrons. This has implications for models of heavy-ion collisions such as the hadron resonance gas model.

One more application is to the viability of resummation of the weak coupling series at high temperature using dimensional reduction. This is possible only if the lowest screening mass belongs to the glue sector [6]. It turns out that dimensional reduction does not work just above the chiral cross over temperature,  $T_c$ .

Hadron-like screening masses have been studied extensively [7, 8]. In QCD with light dynamical quarks they have been studied before using 2 flavours of staggered quarks [9] and with 2+1 flavours of p4 improved quarks [10]. They

---

\*Electronic address: debasish@theory.tifr.res.in

†Electronic address: gavai@tifr.res.in

‡Electronic address: sgupta@theory.tifr.res.in

have been studied also with overlap valence quarks and staggered sea quarks [11]. In all these studies the renormalized light quark masses are almost equal, and nearly physical.

In this work, we extend previous studies through the analysis of meson-like spatial correlation functions in 2-flavour QCD with staggered quarks. This brings the state of the art for dynamical staggered quarks into the regime of lattice spacings already reached using quenched overlap quarks. The organization of our paper is the following: In Section II we discuss operators selected for our analysis and the technical details of our fitting methodology. We investigate chiral symmetry restoration through the correlation functions in Section III. Our results on the screening spectrum are presented in Section IV along with a finite volume analysis. Finally we summarize the main details in Section V. A technical point about the covariances of measurements of correlators is dealt with in Appendix A.

## II. CONFIGURATIONS, MEASUREMENTS AND ANALYSIS

A large part of this study uses decorrelated gauge configurations described in [13]. Two light flavours of staggered quarks were used with the bare quark mass tuned so as to give  $m_\pi \simeq 230$  MeV at zero temperature. The lattice spacing was  $a = 1/(6T)$ , *i.e.*,  $N_t = 6$ . The extraction of the temperature scale was explained in [13]; we note that  $T_c$  was identified there through the peak of the Polyakov loop susceptibility. The lattice volumes,  $V = (aN_s)^3$  were set using  $12 \leq N_s \leq 24$ , *i.e.*, the aspect ratio  $\zeta = T\sqrt[3]{V} = N_s/N_t$  between 2 and 4. This provided basic control of finite volume effects; most of our results are reported for the largest volumes,  $\zeta = 4$ . In addition, we performed a detailed finite volume scaling study at  $T = 0.94T_c$ . For this we generated configurations with  $4/3 \leq \zeta \leq 5$ , with all other parameters fixed as before. We measured autocorrelation times as before, and used at least 50 decorrelated configurations for our measurements.

The meson screening correlation functions projected to zero momentum are—

$$C_z^\gamma = \frac{1}{\mathcal{V}} \left\langle \sum_{\mathbf{x}} \text{Tr} [G(\mathbf{x}, z) G^\dagger(\mathbf{x}, z)] \phi_\gamma(\mathbf{x}) \right\rangle \quad (1)$$

where  $\mathbf{x}$  stands for sites labelled by the triplet  $(x, y, t)$ , the number of terms in the sum is the same as the volume of such a slice,  $\mathcal{V} = N_x N_y N_t$ ,  $G(\mathbf{x}, z)$  is the inverse of the Dirac operator, *i.e.*, the quark propagator from the origin to the point  $(\mathbf{x}, z)$ , the angular brackets denote an average over gauge field configurations with the correct weight, and the staggered phase factors  $\phi_\gamma(\mathbf{x})$  pick out the quantum numbers,  $\gamma$ , of the meson under study.

In this work we have taken all eight possible local staggered phases. At  $T = 0$  they would correspond to the flavour non-singlet scalar (S) (corresponding to the  $a_0$  meson), the Goldstone pion (PS), and three components each of the local vector meson (V) and the axial vector (AV). Symmetry operations of the spatial slice interchange the components of the V and AV, so the three components are expected to be identical after averaging over gauge configurations.

Since we measure spatial direction correlators at finite temperature, the symmetries of the  $(x, y, t)$  slice orthogonal to the direction of propagation are not the same as they would be in the corresponding zero temperature computation [14]. The S/PS operators both lie in the trivial representation, called the  $A_1^{++}$ , of the spatial direction transfer matrix. The sum of the  $x$  and  $y$  polarizations of the V/AV, and, separately, the  $t$  polarization, also lie in the  $A_1^{++}$  representation. These six different kinds of  $A_1^{++}$  operators do not mix under the symmetries of the  $(x, y, t)$  slice, and hence we need separate notations for them. For the S/PS correlators it is economical to carry on the  $T = 0$  notation. For the sum of the  $x$  and  $y$  polarizations of the V we use the notation Vs (and AVs for the sum in the AV sector) and for the  $t$  polarizations we use the notation Vt and AVt. The difference of the  $x$  and  $y$  polarizations of the V/AV lie in a non-trivial representation called the  $B_1^{++}$ . We use the notation VB and AVB for these. These particular realizations of the  $B_1^{++}$  correlator have earlier been seen to vanish [16].

We will also have occasion to use the S and PS susceptibilities [15] defined as

$$\chi_{PS} = \sum_z C_z^{PS}, \quad \text{and} \quad \chi_S = \sum_z (-1)^z C_z^{PS}. \quad (2)$$

The construction uses a fact that we demonstrate later: at high temperatures the S/PS correlators are essentially dominated by a single parity state.

The inversion of the Dirac operator was done using a conjugate gradient (CG) algorithm, as usual. The tolerance for stopping was chosen such that the residual vector had squared norm less than  $\epsilon N_t N_s^3$ . We investigated whether we had an acceptable stopping criterion by monitoring

$$\delta(\epsilon) = 1 - \frac{C^{PS}[\epsilon]}{C^{PS}[\epsilon']} \quad (3)$$

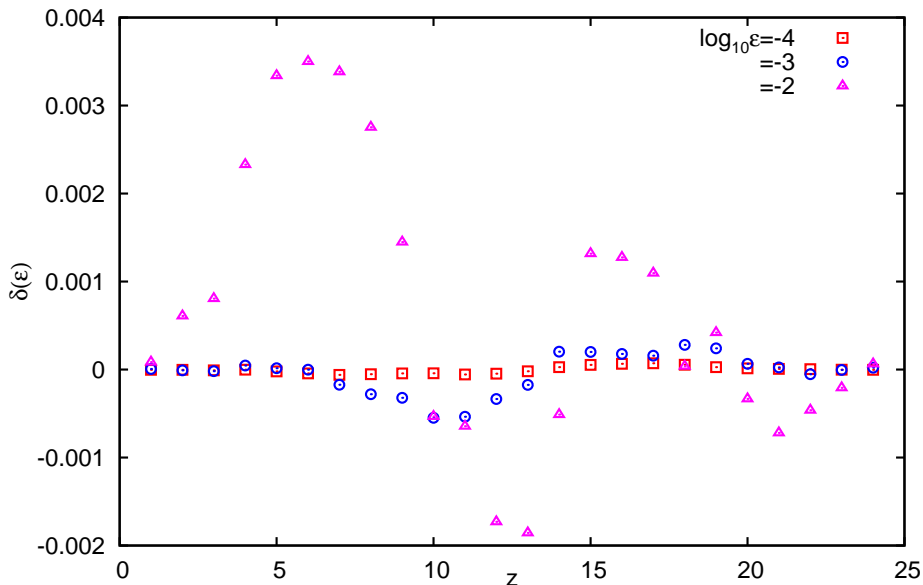


FIG. 1:  $\delta(\epsilon)$ , see eq. (3), as a function of the separation  $z$  for varying  $\epsilon$ , with a fixed value of  $\epsilon' = 10^{-5}$ .

where  $C^{PS}[\epsilon]$  is the PS correlation function obtained when the stopping tolerance parameter is  $\epsilon$ . We chose a fixed  $\epsilon' = 10^{-5}$ . In Figure 1 we show  $\delta$  computed on a randomly chosen test configuration at  $T = 0.94T_c$  with  $\zeta = 4$ . The configuration to configuration variance of  $C^{PS}$  is about 2–5% of the expectation value, so keeping  $\delta < 0.01$  suffices. Clearly, the errors converge fast, and our choice of  $\epsilon = 10^{-5}$  is seen to be more than sufficient.

Each staggered correlation function may contain contributions from two parity partners, and can be parametrized through the doubled-parity fit

$$C(z) = A_1(e^{-\mu_1 z} + e^{-\mu_1(N_z - z)}) + (-1)^z A_2(e^{-\mu_2 z} + e^{-\mu_2(N_z - z)}), \quad (4)$$

where  $\mu_1$  and  $\mu_2$  are the screening masses of the lightest natural parity meson appropriate for the operator used and its opposite parity partner.

Since measurements of the correlation function at different distances,  $z$ , are made using the same gauge configurations, they are correlated, and the fit must take care of these correlations. Therefore, we used the definition of  $\chi^2$

$$\chi^2 = \sum_{zz'} [C_z - C(z)] \Sigma_{zz'}^{-1} [C_{z'} - C(z')]. \quad (5)$$

Here  $z$  is the spatial separation,  $C_z$  are the measured expectation values of eq. (1), the function  $C(z)$  is the 2-mass form of eq. (4), and  $\Sigma_{zz'}$  is the covariance of  $C_z$  and  $C_{z'}$ . When  $\Sigma_{zz'}$  is diagonal, the definition reduces to the more familiar one. In actuality, the correlation coefficients are fairly high, so the matrix  $\Sigma_{zz'}$  is nearly singular. The inversion was done in Mathematica to an accuracy of  $\mathcal{O}(10^{-10})$ . The errors in the inversion were therefore negligible compared to the statistical errors in the measurements,  $\sigma_z$ , which were of the order of a few percent. See Appendix A for further discussion of this procedure.

A check on the consistency of the results obtained from fits is to use local masses. Due to the even-odd oscillations for staggered fermions, we used the definition of [9]—

$$\frac{C_{z+1}}{C_{z-1}} = \frac{\cosh[-m(z)(z+1 - N_z/2)]}{\cosh[-m(z)(z-1 - N_z/2)]}. \quad (6)$$

Given the measurement on the left, the effective mass,  $m(z)$ , can be extracted by solving the equation and errors estimated by jack-knife. This differs from a procedure where successive time slices are used for the modified correlator  $(-1)^z C_z$  [10].

In the chiral symmetry broken phase there is no particular relation between  $\mu_1$ ,  $\mu_2$  and  $A_1$ ,  $A_2$  for different correlators. However, when chiral symmetry is restored, the staggered phases give

$$C_z^{PS} = (-1)^z C_z^S, \quad C_z^{AVs} = (-1)^z C_z^{Vs}, \quad C_z^{AVt} = (-1)^z C_z^{Vt}. \quad (7)$$

This implies the relations

$$A_1^{Vs} = A_2^{AVs}, \quad \mu_1^{Vs} = \mu_2^{AVs} \quad \text{and} \quad (Vs \leftrightarrow AVs), \quad (8)$$

and similarly for the Vt and AVt or the S and PS channels. These relations are very easily demonstrated by using the projections

$$C_z^{(\pm S)} = C_z^{PS} \pm (-1)^z C_z^S, \quad C_z^{(\pm Vs)} = C_z^{Vs} \pm (-1)^z C_z^{AVs}, \quad C_z^{(\pm Vt)} = C_z^{Vt} \pm (-1)^z C_z^{AVt}. \quad (9)$$

If the correlators  $C_z^{(-\gamma)}$  vanish for all  $z$  then chiral symmetry is restored for the full spectrum of excitations.

### III. THERMAL EFFECTS AND APPROXIMATE CHIRAL SYMMETRY RESTORATION

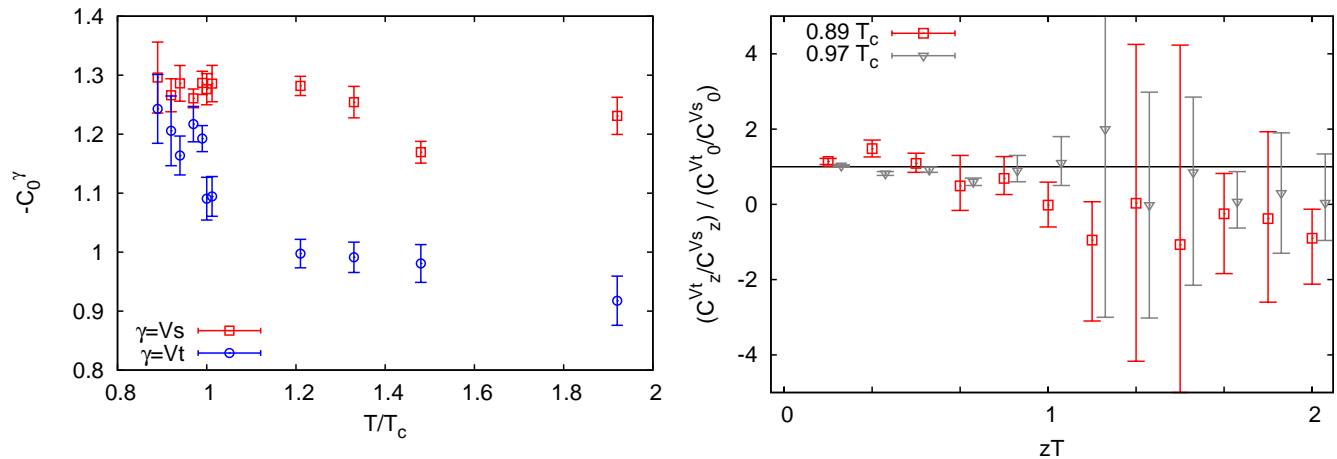


FIG. 2: The panel on the left shows Vs and Vt correlators at  $z = 0$  as a function of  $T/T_c$ . Note the abrupt lifting of the degeneracy at  $T_c$ . The panel on the right shows the ratio of the Vs and Vt correlators as a function of  $z$ , normalized by their values at  $z = 0$ . The data at  $T = 0.97T_c$  is displaced slightly to the right for clarity.

The screening correlators at any non-zero temperature should be decomposed according to the symmetry group of the finite temperature slice. At sufficiently low temperature, however, one expects the Vt and Vs correlators to be nearly equal, and the symmetries of the  $T = 0$  problem to be realized approximately. We investigated this by computing the ratios of the Vt and Vs correlators (normalized to be unity at  $z = 0$ ). The statistical analysis was performed using a bootstrap, since the distribution of the ratio is not expected to be Gaussian [13]. The results below  $T_c$  are shown in Figure 2; the ratio is consistent with unity at all  $z$ . The normalization is the value of the ratio of the correlators at  $z = 0$ . In Figure 2 we have plotted  $C_0^{Vs}$  and  $C_0^{Vt}$  as a function of  $T$ . Below  $T_c$  the two are equal within statistical errors. The two facts taken together imply that the  $T = 0$  symmetries remain good until rather close to  $T_c$ . Quite abruptly, just above  $T_c$  this higher symmetry is broken, and the symmetry of the finite temperature problem is obtained. Similar results are obtained for the AVs and AVt. In view of this, in most of our subsequent analysis, we will group the correlators below  $T_c$  into S, PS, V and AV. For  $T \geq T_c$  we will continue to use the decomposition into S, PS, Vs, Vt, AVs and AVt.

The next question which we examine is whether the correlation functions exhibit chiral symmetry restoration at any temperature. As discussed earlier, the most straightforward way to examine this is to plot  $C_z^{(-\gamma)}$  at each  $T$  and ask whether it is consistent with zero at all  $z$ . In Figure 3 we show these quantities at two temperatures above  $T_c$ . From the correlator  $C_s^{(-S)}$  we see that at  $T = 1.48T_c$  the symmetry is clearly restored, whereas for  $T = 1.012T_c$  the symmetry is broken. The correlator  $C_z^{(-Vs)}$  is consistent with zero for  $zT > 1$ , but at distances less than  $1/T$  there is clear chiral symmetry breaking close to  $T_c$ . The correlator  $V_z^{(-Vt)}$  most nearly exhibits chiral symmetry restoration immediately above  $T_c$ , with only the value at  $z = 0$  being significantly non-zero. At higher temperatures all the  $C_z^{(-\gamma)}$  are consistent with zero at all  $z$ , thereby indicating chiral symmetry restoration.

In order to extend this analysis to all temperatures it is useful to introduce a less local quantity,

$$\chi_\gamma^2 = \sum_{zz'} C_z^{(-\gamma)} \Sigma_{zz'}^{-1} C_{z'}^{(-\gamma)}, \quad (10)$$

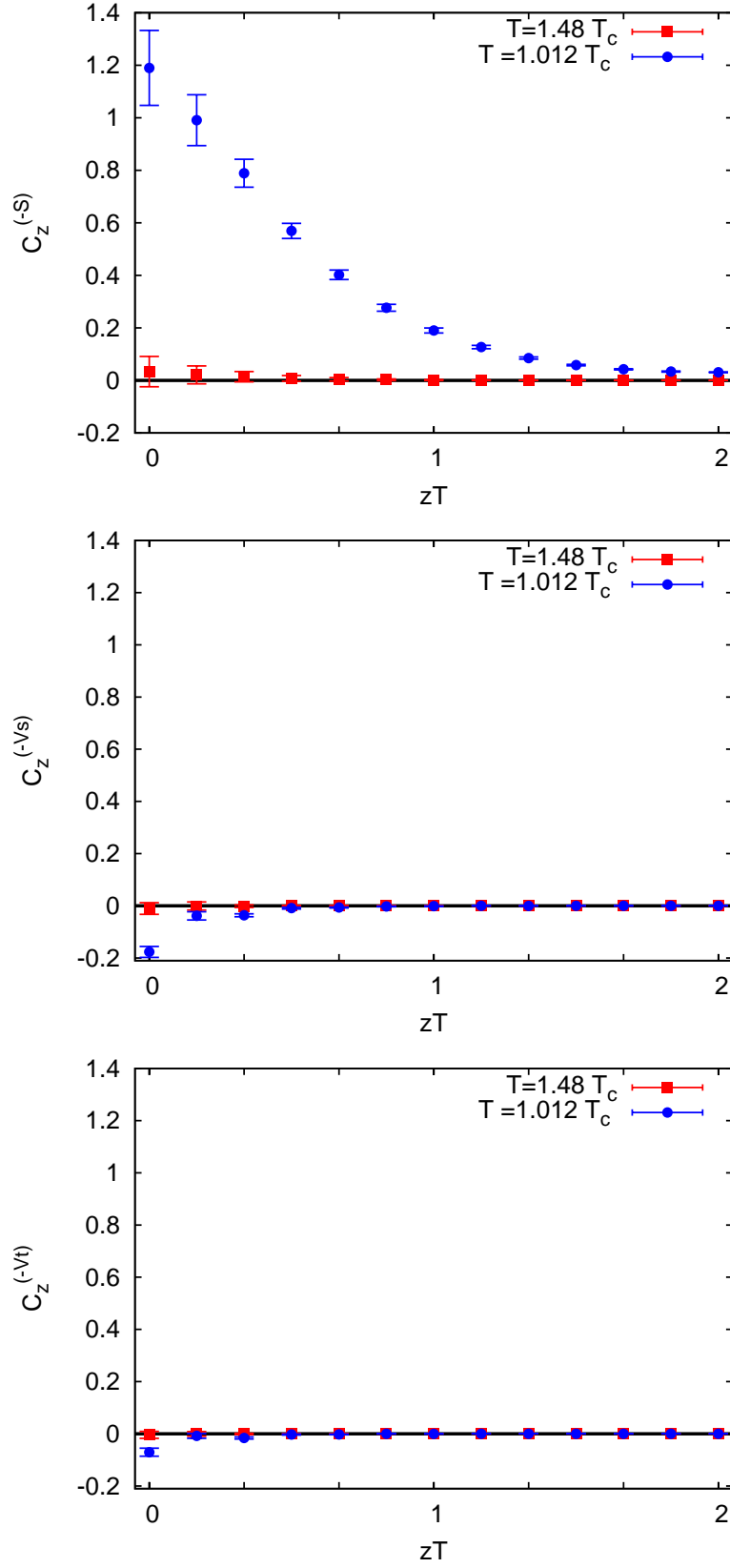


FIG. 3: The chiral projections  $C_z^{(-S)}$ ,  $C_z^{(-Vs)}$  and  $C_z^{(-Vt)}$  of eq. (9) at two temperatures as computed on lattices with  $\zeta = 4$ . The Vt channel shows chiral symmetry is close to being restored immediately above  $T_c$ .

$T/T_c$	$\chi_S^2$	$\chi_{V_s}^2$	$\chi_{V_t}^2$	$\chi_{VB}^2$	$\chi_{AVB}^2$
1.92	0.52	0.42	0.86	16.2	16.2
1.48	9.62	1.33	0.77	10.2	11.5
1.33	13.5	2.07	1.13	14.1	11.7
1.21	441	27	15	19.8	8.8
1.012	1429	107	40	6.2	12.1
1.00	878	125	56	19.0	9.1
0.99	3009	214	114	10.1	17.2
0.97	3013	440	212	14.0	9.2
0.94	746	188	92	28	14.9
0.92	936	348	141	15.0	14.5
0.89	539	101	80	21.3	18.8

TABLE I: This table lists the values of  $\chi^2$  at different temperature for tests of the hypotheses that various correlators vanish. The number of degrees of freedom in all these cases is 12, since there are 13 independent values of  $z$  on the lattices with  $\zeta = 4$  with periodic boundary conditions. In order to rule out the hypothesis that a correlator vanishes at the 99% CL, the value of  $\chi^2$  should be more than 36.

where  $\Sigma_{zz'}$  is the covariance matrix of the measurements of the correlator at different distances. This is a measure of the likelihood that the correlators at all  $z$  are consistent with zero, and hence that chiral symmetry is restored. Values of these variables are collected in Table I. Note that  $\chi_{V_t}^2$  shows a distinct change at  $T_c$ , although it is consistent with chiral symmetry restoration only at  $T = 1.21T_c$ .  $\chi_{V_s}^2$  also shows a change at  $T_c$ , although it is less dramatic. From Figure 3 it would appear that the change in  $\chi_{V_s}^2$  at  $T_c$  is due to the long distance ( $z > 1/T$ ) correlation function becoming consistent with zero, whereas the short distance ( $z \leq 1/T$ ) part disappears only at larger  $T$ .  $\chi_S^2$ , on the other hand, does not seem to undergo any significant change at  $T_c$  and signals chiral symmetry restoration only at  $T = 1.33T_c$ . One sees the difference in behaviour in Figure 3; the S/PS correlators, unlike the V/AV, do not show any kind of effective long distance chiral symmetry restoration. This spatial structure has not been noticed before, and could be worth further investigation in future.

The late restoration of chiral symmetry breaking can be understood from the fact that the non-vanishing quark mass provides explicit chiral symmetry breaking. In the chiral limit, there is a phase transition at  $T_c$ . In the high temperature phase there is, effectively, a single scale,  $T$ , so the screening mass  $\mu \propto T$ . However, when there is a non-vanishing bare quark mass,  $m$ , there is no phase transition at  $T_c$  but only a cross-over. In the absence of a phase transition, one could have  $\mu/T = f(m_\pi/T)$  where  $m_\pi$  is the pion mass at  $T = 0$  (we have traded the bare quantity  $m$  for a renormalized measure of chiral symmetry breaking,  $m_\pi$ ). At large  $T$ , when the argument of the function becomes small,  $f$  should go to a constant. On lowering  $T$  from large values, non-constant behaviour should become visible when the argument becomes of order unity, i.e., at  $T/T_c \simeq m_\pi/T_c$ . Since our simulations are performed with  $m_\pi \simeq 230$  MeV and  $T_c \simeq 175$  MeV, this argument implies that explicit chiral symmetry breaking should manifest itself up to  $T \simeq 1.35T_c$ , which is what we see. Such an argument would lead us to expect that in the real world chiral symmetry breaking in screening masses should not be visible above  $T_c$ . This may have some bearing on the relation between  $T_c$  defined through susceptibilities of the deconfinement and chiral order parameters [17]. An alternative explanation of the late restoration of chiral symmetry is due to approximate restoration of the  $U_A(1)$  symmetry [10]. A future computation with different sea quark masses can easily distinguish between these two alternatives.

The projection of the local V and AV channel correlators on the  $B_1^{++}$  channel is expected to vanish. This was demonstrated in [9, 16] with lattice spacing  $a = 1/(4T)$ . Here we investigate the vanishing of these correlators at smaller lattice spacing using a correlated  $\chi^2$  definition similar to that above. In  $\chi_{VB/AVB}^2$  the factors of  $C_z^{-\gamma}$  in eq. (10) are replaced by the VB or AVB correlator. The results are collected in Table I and show that the VB and AVB correlators vanish.

In Figure 4 we show the ratio of the PS and S susceptibilities (see eq. 2). As expected, they become equal at  $T = 1.33T_c$ , which is the point where the two correlators begin to satisfy eq. (7). At lower temperatures  $\chi_{PS}$  is larger, essentially because  $\mu_{PS}$  is smaller than  $\mu_S$ .

In the next sections we examine the other projection of the correlation function,  $C_z^{(+\gamma)}$ . This is non-zero at all temperatures. At high enough temperature one might expect the whole correlation function to be described in a weak-coupling theory. In Figure 5 we show the correlators at  $T = 1.92T_c$ . One sees that the correlation function is far from the free field theory result, especially the correlator  $C_z^{(+S)}$ ; indicating that even at this temperature the theory cannot be treated as weakly interacting. This is consistent with previous observations [9–11].

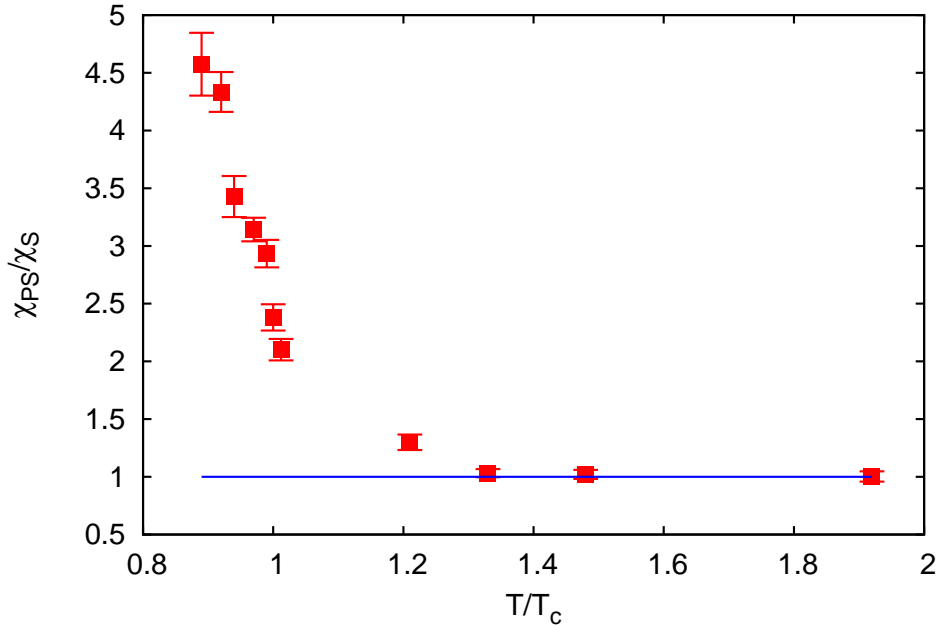


FIG. 4: The ratio for susceptibilities of the pion to the scalar meson.

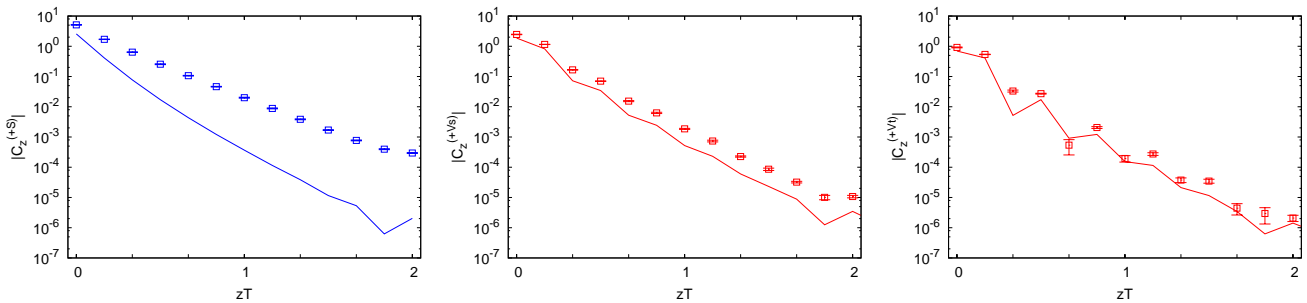


FIG. 5: The correlators  $C_z^{(+\gamma)}$  obtained at  $T = 1.92T_c$  with bare quark mass  $m/T = 0.1$ . The lines show the result for free field theory computed with the same quark mass.

#### IV. SCREENING MASSES

Figure 6 displays all four screening correlators at two temperatures, one each in the hadron and the plasma phase, *i.e.*, at  $T = 0.97T_c$  and  $T = 1.92T_c$ . The V/AV correlators show clear even-odd oscillations at both temperatures, whereas these staggered artifacts are less clear in the S/PS correlators. This has clear implications for the fits: the former always requires a doubled-parity fit of the form given in eq. (4), whereas for the latter a single parity form may suffice.

In Table II we show that this is indeed correct. In the PS channel a single mass fit is acceptable judging by the value of  $\chi^2/\text{DOF}$ , and the fitted value does not change significantly when a doubled-parity fit is performed. In fact, when a doubled-parity fit is attempted to the data, the mass of the parity partner is ill-determined. In the V channel, on the other hand, the doubled-parity fit turns out to be indispensable. In the AV channel the behaviour is similar to that in the V. In the S channel a single mass suffices, although one needs a  $(-1)^z$  factor multiplying the exponential to take care of staggered oscillations. Only at the highest temperature were we able to extract a second mass from the S/PS correlators. The table also shows that the fitted masses are reasonably stable against changes in the fit range in both the PS and V channels. We find similar results for all  $T$ .

Interestingly, although the covariance matrix is nearly singular (the smallest correlation coefficient being about

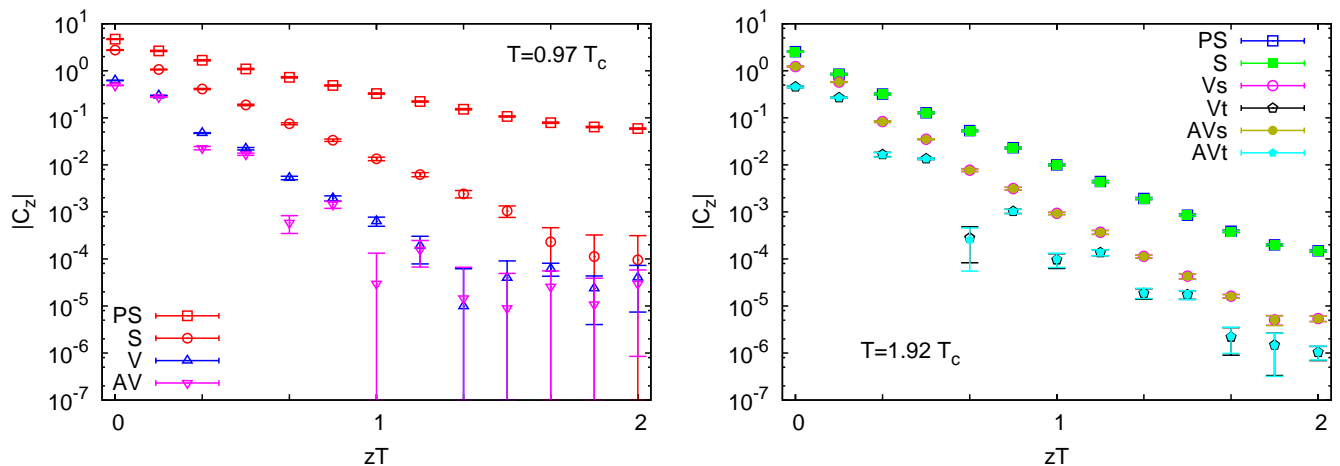


FIG. 6: The correlators for all the mesons at representative temperatures in the two phases on the lattice with  $\zeta = 4$ . Note the absence of even-odd oscillations for the S and PS correlators.

	PS				V		
	Uncorrelated single parity fit						
Range	3-11	4-11	5-11		4-9	4-10	
$A$	3.61(7)	3.59(6)	3.59(6)				
$m$	0.401(2)	0.400(2)	0.400(2)				
$\chi^2/\text{DOF}$	0.24/7	0.01/6	0.01/5				
	Correlated single parity fit						
$A$	3.64(18)	3.59(16)	3.58(16)		0.053(4)	0.053(3)	
$m$	0.401(3)	0.400(3)	0.400(2)		0.484(7)	0.480(8)	
$\chi^2/\text{DOF}$	11.0/7	2.1/6	1.9/5		9.5/4	9.8/5	
	Correlated doubled-parity fit						
		4-11	5-11	6-11	2-11	1-10	3-9
$A_1$		3.59(14)	3.59(12)	3.58(11)	-0.67(4)	-0.70(3)	-0.55(5)
$\mu_1$		0.400(2)	0.400(2)	0.400(2)	1.18(3)	1.20(3)	1.14(3)
$A_2$		0.02(6)	0.04(12)	3.1(*)	0.38(6)	0.49(4)	1.4(4)
$\mu_2$		0.9(*)	0.9(*)	1.5(*)	1.62(8)	1.71(5)	1.98(11)
$\chi^2/\text{DOF}$		1.60/4	1.58/3	1.28/2	6.55/6	6.56/6	2.20/3

TABLE II: Fits to PS and V Correlators at  $T = 0.97T_c$  on a lattice with  $\zeta = 4$ . An asterisk on a number indicates that the fit value is not determined reliably.

0.8), the difference between the parameters extracted using or neglecting the covariance matrix in the PS channel is marginal. The major difference seems to be that the value of  $\chi^2$  obtained when covariances are neglected are clearly too small for the usual statistical interpretation.

In Figure 7 we demonstrate that the fitted masses agree with the local mass extracted from eq. (6). We draw attention to the fact that the local masses exhibit a very well developed plateau, indicating that the correlation functions of fixed parity can be well described by a single mass. The spatial structure of chiral symmetry restoration shown in Figure 3 is visible also in the local masses at high temperature.

In Table III we collect the results for the fitted masses at all temperatures. We checked in all cases that the local masses for  $z > 1/T$  were compatible with these fits. For the V/AV correlators we also checked that if the fits were restricted to  $z \leq 1/T$  the fit results were generally different. Wherever doubled-parity fits are available, one can look for chiral symmetry restoration by checking whether or not the relations of eq. (8) are satisfied. Consistent with the analysis of Section III, we find that this happens only for  $T \geq 1.33T_c$  in the S/PS channels. Surprisingly, the equalities of eq. (8) hold in the V/AV channels, within statistical errors, from just above  $T_c$ .



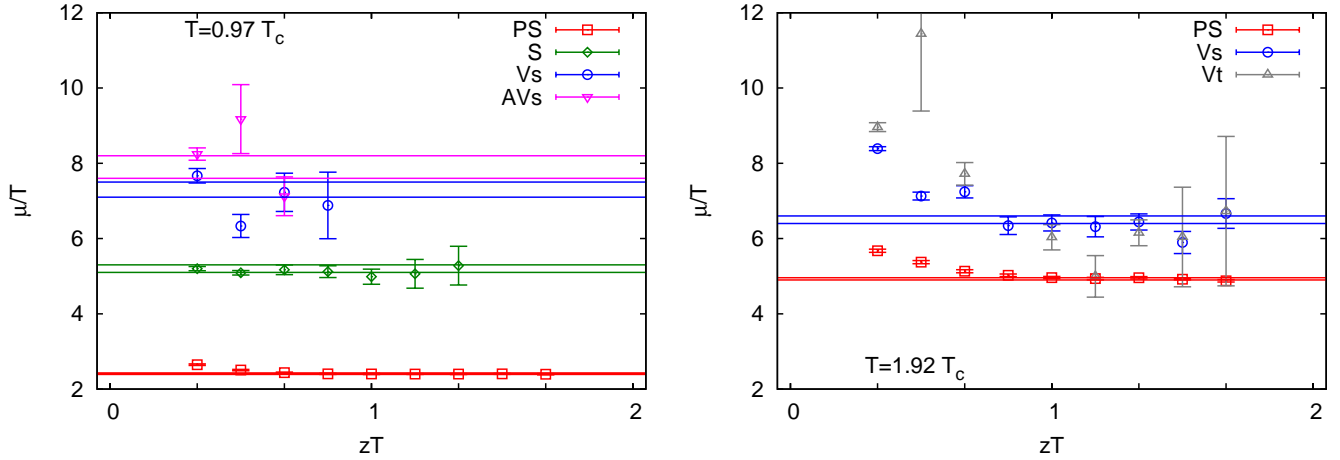


FIG. 7: The extracted local masses for the mesons at representative temperatures in the two phases on a lattice with  $\zeta = 4$ . In the high temperature phase, where chiral symmetry is restored, only the PS, Vs and Vt masses are shown since the S, AVs and AVt exactly coincide.

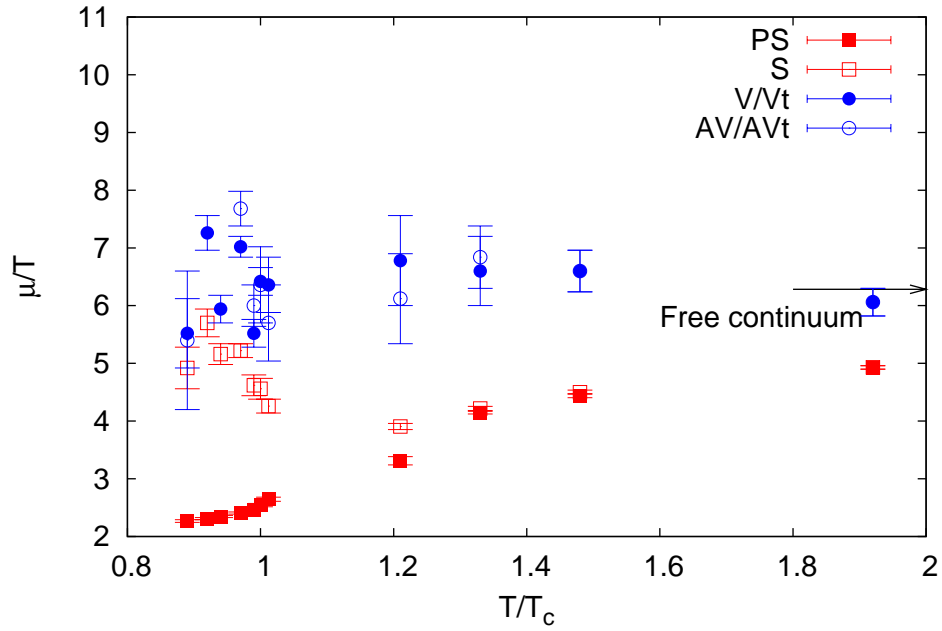


FIG. 8: Screening masses as functions of  $T/T_c$ . Below  $T_c$  the S, PS, V and AV channels are shown. At  $T_c$  and above the S, PS, Vt and AVt are shown. The free continuum value of  $2\pi$  is indicated with an arrow.

In Figure 8 we plot the lowest screening mass in each channel as a function of  $T/T_c$ . Above  $T_c$  we could plot three channels. To avoid clutter we plotted only the S/PS and Vt/AVt channels. As one sees in Table III, the lowest Vs/AVs masses are slightly larger, but consistent with Vt/AVt at the  $2\text{-}\sigma$  level. All the features discussed are clearly visible here. Also visible is the fact that  $\mu_{PS}/T$  increases monotonically with  $T$  whereas  $\mu_S/T$  dips near  $T_c$ . Note also that  $\mu_{Vt}/T$  may approach its ideal gas value from above, becoming consistent with the limit already at  $T \simeq 2T_c$ . However  $\mu_S/T$  remains about 20% below this limit even at the highest temperature we explored. We shall return to this point later when we discuss the continuum limit.

$T/T_c$		PS	S	Vs	AVs	Vt	AVt
1.92	$\mu_1/T$	4.93(3)	5.1(6)	6.5(1)	12.6(4)	9.4(3)	6.1(2)
	$\mu_2/T$	5.1(7)	4.93(3)	12.8(4)	6.5(1)	6.1(2)	9.3(4)
	$\chi^2$	15.8	16	9.2	9.3	7.4	7.2
1.48	$\mu_1/T$	4.44(4)	17(1)	6.8(1)	5.8(4)	8.9(4)	6.6(4)
	$\mu_2/T$	—	4.5(4)	5.6(4)	6.8(1)	6.6(4)	8.7(4)
	$\chi^2$	8.1	1.8	5.2	5.3	9.6	9.2
1.33	$\mu_1/T$	4.15(2)	7.0(7)	6.7(2)	9.6(6)	8.7(3)	6.8(5)
	$\mu_2/T$	—	4.22(4)	8.7(5)	6.8(2)	6.6(6)	8.9(4)
	$\chi^2$	31.8	9.2	11.4	11.3	6.0	7.7
1.21	$\mu_1/T$	3.31(7)	—	6.5(2)	9.4(8)	8.1(4)	6.1(8)
	$\mu_2/T$	—	3.91(5)	15.0(6)	6.8(2)	6.8(8)	9.1(4)
	$\chi^2$	18.2	6.3	5.4	12.5	2.2	3.8
1.012	$\mu_1/T$	2.65(4)	23(3)	6.9(3)	4.5(9)	6.4(5)	5.7(7)
	$\mu_2/T$	—	4.3(1)	4(2)	8.8(4)	5(1)	5.3(6)
	$\chi^2$	21.2	7.4	5.2	2.1	1.0	2.8
1.00	$\mu_1/T$	2.54(3)	—	5.9(3)	5.2(6)	7.9(4)	13(2)
	$\mu_2/T$	—	4.6(2)	9.8(9)	8.6(4)	—	11.6(5)
	$\chi^2$	11.9	7.0	6.1	4.6	3.2	7.8
		PS	S	V	AV		
0.99	$\mu_1/T$	2.47(2)	5(1)	5.5(2)	6.4(5)		
	$\mu_2/T$	—	4.6(2)	12(1)	6.0(4)		
	$\chi^2$	8.4	2.6	6.3	4.3		
0.97	$\mu_1/T$	2.41(2)	4(1)	7.0(2)	7.0(3)		
	$\mu_2/T$	—	5.2(1)	11(1)	7.7(3)		
	$\chi^2$	11.0	3.6	6.5	1.7		
0.94	$\mu_1/T$	2.35(2)	4(2)	5.9(2)	4(1)		
	$\mu_2/T$	—	5.2(2)	—	14.4(3)		
	$\chi^2$	15.3	3.2	2.8	2.4		
0.92	$\mu_1/T$	2.31(2)	5(1)	7.3(3)	7.3(7)		
	$\mu_2/T$	—	5.7(2)	—	10.0(7)		
	$\chi^2$	7.5	1.3	6.5	7.6		
0.89	$\mu_1/T$	2.27(2)	—	5.5(6)	7(1)		
	$\mu_2/T$	—	4.9(4)	7(2)	5(1)		
	$\chi^2$	5.6	7.7	4.3	12.2		

TABLE III: Screening masses at different temperatures. The fit range was  $z/a=3-11$  except for the S/PS at  $1.92T_c$ , where the fit range was  $z/a=4-11$  (the larger range gave very large  $\chi^2$  without appreciably changing the best fit values). Also note that except at  $1.92T_c$ , the PS fit was done with a single-parity fit form, and therefore has two more degrees of freedom than the other channels. A dash indicates that some mass could not be obtained because staggered oscillations were not visible. At temperatures below  $T_c$  the analysis was performed on the V/AV channels.

### A. The role of explicit chiral symmetry breaking

In free field theory one has no pion and the explicit chiral symmetry breaking scale is the quark mass. In this case one has

$$\frac{\mu}{T} = 2\sqrt{\pi^2 + \left(\frac{m}{T}\right)^2} \simeq 2\pi \left[1 + \frac{1}{2} \left(\frac{m}{\pi T}\right)^2\right]. \quad (11)$$

Substituting the bare quark mass into this expression, it can be seen that the effect is of the order of a few parts in  $10^5$ , and hence negligible. However, it turns out that in weak-coupling theory one has to insert in the above equation the thermal mass of the quark [18]. Since this is  $gT/\sqrt{3}$ , and  $g$  is large near  $T_c$  [19], the effect can be significant. Of

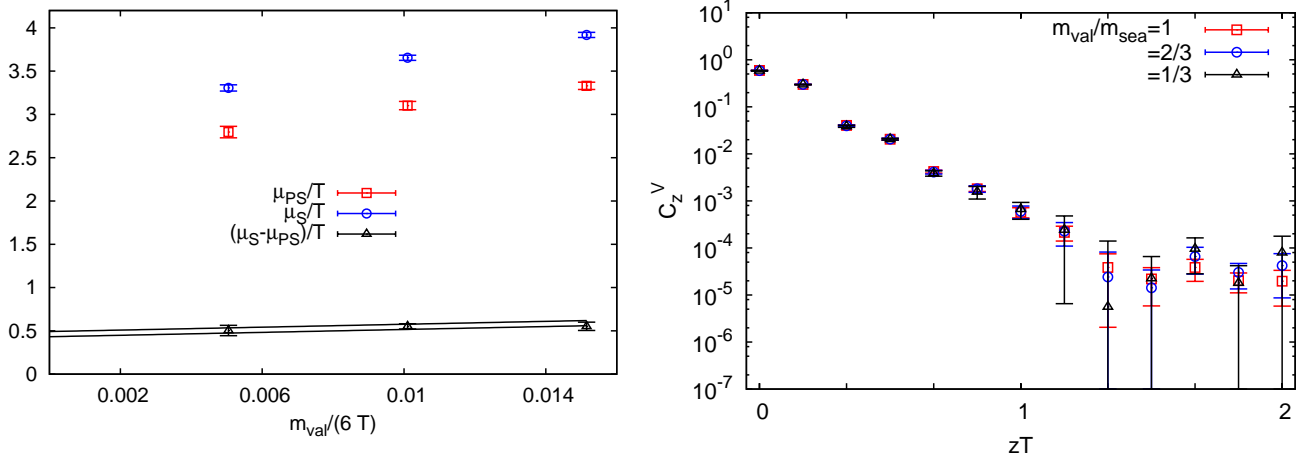


FIG. 9: The valence quark mass dependence of various quantities at  $T = 1.21T_c$  when the bare sea quark mass is held fixed at the value  $m/T_c = 0.1$  (corresponding to  $m_\pi \simeq 230$  MeV). The screening masses in the S/PS sector depend significantly on the valence quark mass, whereas the V sector screening correlators are insensitive.

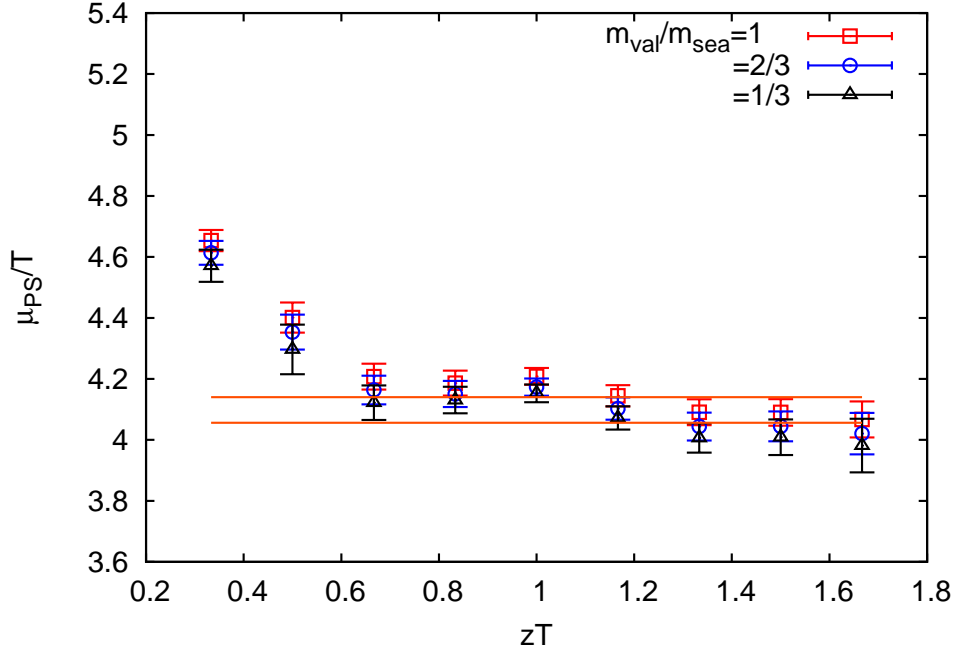


FIG. 10: Local masses in the PS channel for different valence quark masses at  $T = 1.33T_c$  with  $\zeta = 4$ . The horizontal lines are the 1-sigma bounds from the fit to the correlator for  $m_{val} = m_{sea}$ .

course, when  $g$  is large, the weak-coupling theory is unlikely to be quantitatively useful, and should be taken only as an indication that one must explore the quark mass dependence of the chiral symmetry breaking seen in the screening masses.

Changing the quark mass involves in principle a completely new set of computations, and lies beyond the scope of this paper. However, it is possible to change the valence quark mass ( $m_{val}$ ) without changing the sea quark mass ( $m_{sea}$ ). As a result, such a restricted study can be done without a large cost in CPU time. In view of this, we repeated our analysis above  $T_c$  with  $m_{val}$  chosen to be 2/3 and 1/3 of  $m_{sea}$ . Sample results are shown in Figure 9.

We find that a change in the valence quark mass has insignificant effect in the V/AV channels (see, for example, the second panel of Figure 9). However, there are statistically significant changes in the S/PS sector. Both the S and

PS screening mass increase with  $m_{val}$ . The difference also increases, although the limiting value for  $m_{val} = 0$  is finite. We find that

$$\left. \frac{\mu_S - \mu_{PS}}{T} \right|_{T/T_c=1.21} = 0.46 \pm 0.03 \quad (\text{for } m_{sea}/T_c = 0.1, m_{val} = 0). \quad (12)$$

It is not inconceivable that decreasing  $m_{sea}$  in a future computation can lower this mass difference further. Note, however, that  $\mu_{PS}/T$  and  $\mu_S/T$  both drop as the quark mass changes, and move further away from the weak-coupling expectation.

In fact, the dependence of correlation functions on the bare quark mass can be deeper than what was discussed above. We illustrate this in Figure 10, where local masses in the PS channel are shown for several values of  $m_{val}$ . It seems that with decreasing  $m_{val}$  the plateau in the local masses becomes less well developed; for the smallest  $m_{val}$ , in fact, a distinct slope is visible.

### B. The effect of finite volume

$\zeta$		PS	S	V	AV
4/3	$\mu_1$	2.45(4)	—	8.0(2)	4.3(6)
	$\mu_2$	—	5.0(3)	—	7.7(6)
2	$\mu_1$	2.41(2)	—	6.8(3)	13.1(7)
	$\mu_2$	—	5.5(2)	14.7(5)	9.2(5)
3	$\mu_1$	2.44(3)	6(1)	6.5(2)	8.0(3)
	$\mu_2$	—	5.3(2)	6.4(8)	9.1(3)
4	$\mu_1$	2.35(2)	4(2)	6.4(3)	7.6(3)
	$\mu_2$	—	5.2(2)	29(4)	9.4(2)
5	$\mu_1$	2.39(2)	4.2(-)	6.6(4)	8.1(5)
	$\mu_2$	—	5.5(4)	9(1)	8.6(4)

TABLE IV: Screening mass estimates at  $T = 0.94T_c$  at fixed  $a = 1/(6T)$  with changing spatial volume  $(\zeta/T)^3$ .

Finite volume effects in the high temperature phase of QCD have been explored earlier [9] and are by now well understood. These effects are under control as long as  $\mu_{PS}$  is large compared to the inverse size of the smallest lattice dimension, *i.e.*,  $T$ . Since we find  $\mu_{PS}/T > 2.5$  in the high temperature phase, we expect that finite volume effects are under control for  $T > T_c$ .

In this paper we report on the magnitude of finite volume effects, below  $T_c$ . We studied the screening correlators on lattices with  $4/3 \leq \zeta \leq 5$  at  $T = 0.94T_c$ . As shown in Table IV and Figure 11, finite volume effects are invisible within statistical errors. Again, since  $\mu_{PS}/T \simeq 2.3$ , this may not seem unexpected.

It is worth the remark that while such studies can have some bearing on decay widths at finite temperature, much larger lattices and smaller quark masses and lattice spacings may be required for those. For example, the scalar under study cannot decay into two pions, and must have at least three pions in the final state. This is ruled out kinematically at present.

On the other hand, since  $\mu_S/\mu_{PS} \simeq 2.2$ , one must ask whether the long-distance behaviour of the S correlator is determined by a single scalar exchange or multi-particle exchanges (this is the finite temperature analogue of particle decays, and we shall save space by using the word decay). In the continuum theory, this non-isosinglet scalar cannot decay into two pions. From this point of view, since  $\mu_S/\mu_{PS} \simeq 2.2 < 3$ , one could expect that the scalar does not decay. However, with staggered quarks on a lattice, there are spurious two pion states (taste multiplets) through which the scalar current could be correlated [20]. The featureless behaviour of the volume dependence of the screening masses implies that no decays occur. However, this is a weak statement, because a 7% taste symmetry breaking is sufficient to forbid this decay on the largest lattice which we used.

### C. The continuum limit

In Table V we extract the values of the screening masses in units of temperature,  $\mu/T$  for two different temperatures in the chirally symmetric phase, at two different lattice spacings. From two pieces of data in each case it is hard

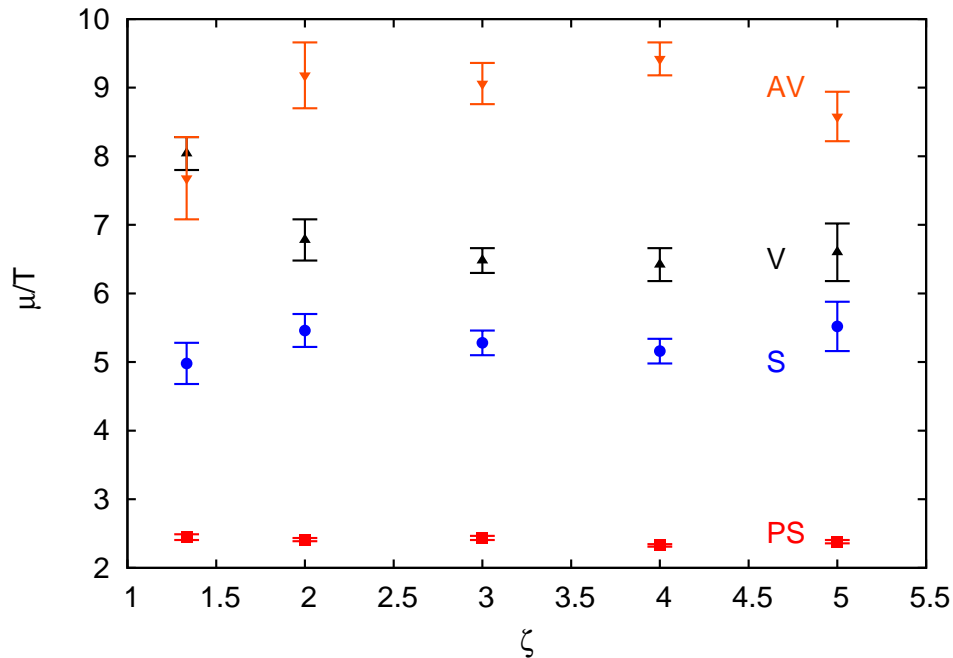


FIG. 11: Screening masses in various channels as a function of  $\zeta$  at  $T = 0.94T_c$ . Note that there is nothing special about the S channel masses.

$T/T_c$	$a = 1/(4T)$		$a = 1/(6T)$	
	S/PS	Vt/AVt	S/PS	Vt/AVt
1.5	$3.67 \pm 0.02$	$5.44 \pm 0.08$	$4.44 \pm 0.04$	$6.6 \pm 0.4$
2.0	$4.08 \pm 0.01$	$5.72 \pm 0.04$	$4.93 \pm 0.03$	$6.1 \pm 0.2$

TABLE V: The lattice spacing dependence of  $\mu/T$  in various quantum number channels. The temperature scale is rounded off. Data for  $a = 1/(4T)$  is taken from [9].

to construct a continuum extrapolation. However, we can test whether the extrapolation is consistent with the expectation  $\mu \simeq 2\pi T$  by attempting a fit to the form

$$\left. \frac{\mu}{T} \right|_{N_t} = 2\pi + \frac{s}{N_t^2}. \quad (13)$$

It is possible to get reasonable fits in the V/AV channel, yielding

$$s = \begin{cases} -13 \pm 2 & (T = 1.5T_c) \\ -9.0 \pm 0.2 & (T = 2T_c) \end{cases} \quad (14)$$

This is consistent with previous results. However, in the S/PS case this procedure fails to yield the expected result; the extrapolated screening length remains below the ideal gas value. One cannot rule out the possibility that the weak-coupling result emerges at even smaller lattice spacings.

We note however, that the screening of meson-like correlations in the weak coupling theory occurs, not through the exchange of a single particle, but through multiparticle exchange. As a result, the zero-momentum correlator is not expected to be strictly exponential, but to have some curvature. Such a curvature was actually seen in computations in the quenched theory using staggered [21] and Wilson [8] quarks using much smaller lattice spacings. An easily observed feature of such a curvature is that local masses do not show a plateau, but change continuously with  $z$ . Such behaviour was neither seen here (see Figure 7), nor with p4 improved quarks at the same renormalized quark mass [10]. However, as pointed out in Section IV A, when the quark mass is lowered such a feature could emerge.

## V. SUMMARY

We studied screening correlation functions and screening masses of meson-like probes of strongly interacting matter, both in the low temperature hadron and high temperature plasma phases. We used configurations described in [13]; these were generated using two flavours of dynamical staggered quarks with masses tuned to give  $m_\pi \simeq 230$  MeV. Most of the results come from lattice spacing  $a = 1/(6T)$ , although we have attempted to check assumptions about the continuum limit using earlier measurements with the same renormalized quark mass and lattice spacing  $a = 1/(4T)$ . We have explicitly checked for finite volume effects, and found that these are negligible when we take the aspect ratio  $\zeta = 4$ .

We checked that the correlators at  $T < T_c$  effectively have the symmetries of the  $T = 0$  transfer matrix, and that there is a fairly abrupt transition at  $T_c$  to the symmetries of the screening transfer matrix (see Figure 2). Although the QCD cross over occurs at  $T_c$ , we found a lack of parity doubling in the spectrum of screening masses up to a temperature of  $1.33T_c$  (see, for example, Figure 4 and Table I). We argued that explicit chiral symmetry breaking due to the quark mass is visible up to a temperature of  $1.35T_c$ , as seen here. This argument leads us to believe that in the limit of realistic quark masses, such a breaking would not be visible above  $T_c$ . Interestingly, there turns out to be a lot of structure in this apparent breaking of chiral symmetry above  $T_c$ . The V/AV correlators are equal to each other at distances  $z > 1/T$ , and the chiral symmetry breaking in this sector is entirely a short distance effect (see Figure 3). In the S/PS sector the non-degeneracy of the correlators persists into the long distance regime.

Non-degeneracy of the S/PS correlators could also be due to  $U_A(1)$  symmetry breaking. This is suspected to persist well into the high temperature plasma phase [22]. We tested what happens to the S/PS difference as the valence quark mass is changed (see Figure 9). Our results imply that other physics effects can be disentangled from the explicit symmetry breaking effect due to finite quark mass only through computations with smaller quark masses. Alternatively, one could examine the short distance part of the V/AV correlators for signals of such microscopic physics.

We made the first study of hadron decays at finite temperature (below  $T_c$ ) through a systematic exploration of the volume dependence of screening masses. We found no significant volume dependence (see, for example, Table IV and Figure 11), indicating the stability of the scalar. As we discussed already, this study needs to be carried out with smaller quark masses so that  $\mu_S/\mu_{PS} > 3$ , or at smaller lattice spacings, so that taste violations are reduced.

We combined the analysis of this paper with data from an earlier source [9] in which the same renormalized quark masses were used to study screening at a coarser lattice spacing,  $a = 1/(4T)$  to explore the continuum limit. Being restricted to only two values of the lattice spacing at each  $T$ , we ask whether the continuum limit of screening masses is compatible with the ideal gas expectation,  $2\pi T$ , in the high-temperature phase. We find that it is, in the V/AV channels, but not in the S/PS channels.

If the high temperature phase is deconfined, then correlations of static currents with meson quantum numbers must be mediated by the exchange of a quark anti-quark pair. The most straightforward signal of this is that the local masses do not show a well-developed plateau. In most of our studies we did not see this. Only in a study with rather small valence quark masses did we see a signal of such behaviour (see Figure 10). Studies with lower sea quark masses in the future will be needed to resolve the question of deconfinement above  $T_c$  in QCD with physical quark masses.

## Acknowledgments

The computations were performed on the CRAY X1 of the Indian Lattice Gauge Theory Initiative (ILGTI) in TIFR, Mumbai. We thank Ajay Salve and Kapil Ghadiali for technical support. DB wishes to acknowledge useful discussions with Saumen Datta, Nilmani Mathur and Jyotirmoy Maiti.

## Appendix A: Covariance matrices and statistical data compression

The correlation functions are evaluated on a fixed set of gauge configurations. In general, the estimates of the correlator at different separations are not statistically independent. The covariance matrix of the correlators measures the degree of independence, and is defined as

$$\Sigma_{zz'} = \langle (C_z^\gamma - \langle C_z^\gamma \rangle) (C_{z'}^\gamma - \langle C_{z'}^\gamma \rangle) \rangle, \quad (\text{A1})$$

where the averages are over the ensemble of gauge configurations. The diagonal elements are the variances. The matrix is positive and symmetric by construction, so that it has well defined (positive) eigenvalues and orthogonal

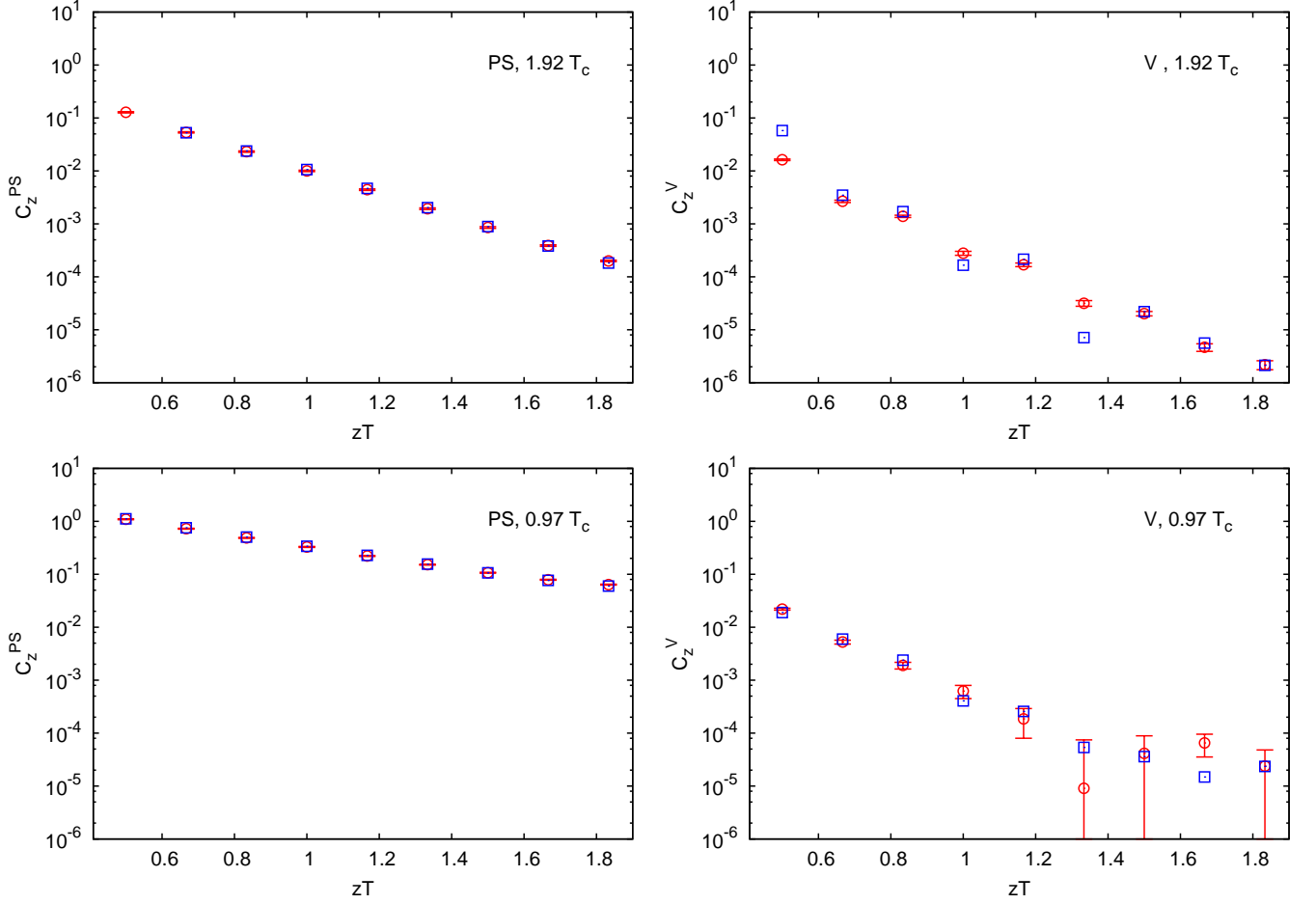


FIG. 12: The measured correlator (red circles) and the compressed version obtained by projection on to a single eigenvector of  $\Sigma$  (blue squares) for the PS and V at  $T = 1.92T_c$  and  $0.97T_c$ .

eigenvectors. It is found that it often has large condition number, *i.e.*, the ratio of the largest and smallest eigenvalues is large. Any fits to the correlation function are made by minimizing the  $\chi^2$ -function

$$\chi^2 = D^t \Sigma^{-1} D, \quad \text{where} \quad D = C^\gamma - f, \quad (\text{A2})$$

$C^\gamma$  is the vector of measured correlation functions, with components  $C_z^\gamma$ , and  $f$  is the corresponding vector made from the function to be fitted.

The covariance matrix is often inverted using a singular value decomposition,  $\Sigma = UDV^T$  where  $U$  and  $V$  are orthogonal matrices (in this case  $U = V$ ) and  $D$  is diagonal. The inverse matrix is usually obtained as  $\Sigma^{-1} = VD^{-1}U^T$ , with the largest components of  $D^{-1}$  set to zero [23]. This procedure is used to prevent errors arising from finite precision rounding. For this part of the analysis we use Mathematica, which allows arbitrary precision computations. By tuning the precision of the computation from 10 digits to 40 digits, we checked for control of rounding errors. Our conclusion is that the rounding errors can be kept under control without setting large numbers to zero. As a result, in our ensuing investigations we are assured that the eigenvalues of  $\Sigma$  are the inverses of those of  $\Sigma^{-1}$ .

The covariance matrix and its eigenvectors are determined essentially by the statistical properties of the measurement and not directly by the correlation function. One extreme can be illustrated by the imagined case where we generate a very large set of decorrelated gauge configurations, and use a disjoint subset for evaluation of the correlator at each  $z$ . Since the measurements at each of the  $z$  are then statistically independent of each other,  $\Sigma$  must be diagonal. As a result, the eigenvectors have support only on a single separation  $z$ .

Take the eigenvalues of  $\Sigma^{-1}$  to be  $\lambda_\alpha$  with corresponding eigenvectors  $v_\alpha$ . Each correlation function can be written

as a linear combination of the  $v_\alpha$ , *i.e.*,

$$C^\gamma = \sum_\alpha c_\alpha^\gamma v_\alpha. \quad (\text{A3})$$

Our purpose in doing this is that if some of the  $c_\alpha^\gamma$  turn out to be small then one can perform a noise reduction by dropping the small terms. Since  $c_\alpha^\gamma = C^\gamma \cdot v_\alpha$ , the errors on the dot product are clearly given by

$$\sigma^2(c_\alpha^\gamma) = v_{\alpha z} v_{\alpha z'} \Sigma_{zz'} = \frac{1}{\lambda_\alpha}. \quad (\text{A4})$$

In writing this formula we have taken  $v_{\alpha z}$  to have no errors. This approximation can be removed, if necessary, by a bootstrap analysis of the errors in  $c_\alpha^\gamma$ . If many of the components,  $c_\alpha^\gamma$ , are zero within errors, then we can drop them from the analysis. In this case we say that the correlation function is compressible. Such a notion corresponds to that of ‘lossy data compression’ in a variety of contexts, including jpeg image compression and mp3 audio compression.

In the imagined case which we discussed before, generically all the  $c_\alpha^\gamma$  will be non-zero and the correlator will not be compressible. Only if some of the measurements are so noisy that they are compatible with zero can we drop them from the fits. This example illustrates the connection of compressibility with that of statistical independence.

The actual situation we investigated was the usual one where the correlation function at all separations were measured on all configurations and the lowest mass was obtained by a fit to the long-distance correlation function using the cuts mentioned in Section IV, *i.e.*,  $3 \leq z/a \leq 13$ . Very surprisingly, we found that the PS correlator can be compressed to exactly one component, corresponding to the smallest  $\lambda_\alpha$  both above and below  $T_c$ . This means that the corresponding eigenvector  $v_\alpha$  contains the full information on the correlator. The V correlator can also be compressed down to a very small number of components, usually one or two. These surprising results are shown in Figure 12. When we examine the correlation functions at all distances, then again we find a high, but lesser, degree of compressibility with two or three eigenvectors being needed for the description of the data.

What is the origin of these extremely strong covariances in the data? The gauge configurations we used were chosen so that thermodynamic operators such as the action, Polyakov loops, chiral condensate, various quark number susceptibilities, are decorrelated between one configuration and another. Several of these quantities, for example, those which involve fermions, are highly non-local. In view of this, autocorrelations between configurations are not the cause of the high compressibility of the data.

So it must be the correlation function itself which generates these covariances, with the result that one of the eigenvectors,  $v_\alpha$  contains all the information present in the measured correlator. Could this be due to the fact that the Dirac propagators are highly non-local? If so, the baryon correlators must also be highly compressible, whereas glueball correlators need not be. Or could it be that the relatively low masses are at the root of the covariance? If so, neither the baryon nor glueball correlators need be compressible. Since correlated fits are standard technology in the fitting of masses, measuring statistical compressibility of correlators is a trivial extension of standard lattice measurements. It would be interesting to have more data in future on the compression of correlation functions.

- 
- [1] C. DeTar and J. B. Kogut *Phys. Rev. D* 36 (1987) 9.
  - [2] O. Kaczmarek, *PoS CPOD07* (2007) 043.
  - [3] K. Kajantie *et al.*, *Phys. Rev. Lett.* 79 (1997) 3130.
  - [4] S. Datta and S. Gupta, *Nucl. Phys. B* 534 (1998) 392.
  - [5] K. D. Born *et al.*, (MT<sub>c</sub> Collaboration) *Phys. Rev. Lett.* 67 (1991) 302.
  - [6] R. V. Gavai and S. Gupta, *Phys. Rev. Lett.* 85 (2000) 2068;  
M. Laine and M. Vespäläinen, *J. H. E. P.* 0909 (2009) 023.
  - [7] C. Bernard *et al.*, (MILC Collaboration) *Phys. Rev. Lett.* 68 (1992) 2125;  
E. Laermann and P. Schmidt, *Eur. J. Phys. C* 20 (2001) 541.
  - [8] S. Wissel, *PoS LAT2005* (2006) 164;  
E. Laermann, *PoS LAT2008* (2008) 193.
  - [9] R. V. Gavai, S. Gupta and P. Majumdar, *Phys. Rev. D* 65 (2002) 054506.
  - [10] M. Cheng *et al.*, arXiv:1010.1216.
  - [11] R. V. Gavai, S. Gupta and R. Lacaze, *Phys. Rev. D* 72 (2008) 014502.
  - [12] D. Banerjee *et al.*, *PoS LAT2010* (2010) 168.
  - [13] R. V. Gavai and S. Gupta *Phys. Rev. D* 78 (2008) 114503.
  - [14] S. Gupta, *Phys. Rev. D* 60 (1999) 094505.
  - [15] S. Gupta, *Phys. Lett. B* 288 (1992) 171.
  - [16] R. V. Gavai and S. Gupta *Phys. Rev. Lett.* 83 (1999) 3784.



- [17] A. Bazavov *et al.* (for the HotQCD Collaboration), arXiv:1009.4914;  
S. Borsanyi *et al.*, arXiv:1011.4230.
- [18] M. Vespäläinen, *J. H. E. P.* 0703 (2007) 022;  
W. M. Alberico *et al.*, *Nucl. Phys. A* 792 (2007) 152.
- [19] S. Gupta, *Phys. Rev. D* 64 (2001) 034507.
- [20] S. Prelovsek, *Phys. Rev. D* 73 (2006) 014506;  
C. Bernard *et al.*, (MILC Collaboration) *Phys. Rev. D* 76 (2007) 094504.
- [21] R. V. Gavai and S. Gupta *Phys. Rev. D* 67 (2003) 034501.
- [22] R. V. Gavai, S. Gupta and R. Lacaze, *Phys. Rev. D* 65 (2002) 094504.
- [23] W. H. Press *et al.*, *Numerical Recipes in C*, Cambridge, 1992.